J Geod (2011) 85:597–605
DOI 10.1007/s00190-011-0462-2

ORIGINAL ARTICLE

Strapdown INS/DGPS airborne gravimetry tests in the Gulf of Mexico

Xiaopeng Li

Received: 25 August 2010 / Accepted: 12 March 2011 / Published online: 26 March 2011

Abstract Combining data from a Strapdown Inertial Navigation System and a Differential Global Positioning System (SINS/DGPS) has shown great promise in estimating gravity on moving platforms. Previous studies on a ground-vehicle system obtained 1–3 mGal precision with 2 km spatial resolution. High-accuracy Inertial Measurement Units (IMU) and cm-level positioning solutions are very important in obtaining mGal-level gravity disturbance estimates. However, these ideal configurations are not always available or achievable. Because the noise level in the SINS/DGPS gravimetric system generally decreases with an increase of speed and altitude of the platform, the stringent constraints on the IMU and GPS may be relieved in the airborne scenario. This paper presents an investigation of one navigation-grade and one tactical-grade IMU for the possibility of low-cost INS/GPS airborne gravimetry. We use the data collected during the Gravity-Lidar Study of 2006 (GLS06), which contains aerogravity, GPS, and INS along the northern coastline of the Gulf of Mexico. The gravity disturbance estimates from the navigation-grade IMU show 0.5–3.2 mGal precision compared with the onboard gravimeter's measurements and better than 3 mGal precision compared with the upward continued surface control data. Due to relatively large (240 s) smoothing window, the results have about 34 km along-track resolution. But the gravity estimates from the tactical-grade IMU have much poorer precisions. Nonetheless, useful contributions from the tactical-grade IMU could be extracted for longer wavelengths.

Keywords Strapdown Inertial Navigation System · Inertial Measurement Unit · DGPS · Gravity

X. Li (✉)
ERT at the National Geodetic Survey,
Silver Spring, Maryland 20901, USA
e-mail: Xiaopeng.Li@noaa.gov

1 Introduction

Global Positioning System (GPS) and Inertial Navigation System (INS) have been integrated primarily for the purpose of navigation and precise kinematic positioning over the past few decades. Both the accuracy and the continuity of the positioning solution are improved by combining the GPS data (either the raw observables or the final positioning solution) with the velocity and angular increments measured by the IMU via various filtering techniques (Li 2007). On the other hand, considering the inverse of the problem, Jekeli (2000) and Schwarz (2006) developed rigorous equations for estimating the full gravity vector based on the computed GPS kinematic acceleration (twice differential of the position with respect to time) and the IMU-measured dynamic acceleration. In the airborne scenario, better than 5 mGal precision in the down component and 6–8 mGal precision in the horizontal components of the gravity disturbance with about 10 km spatial resolution are reported by Kwon and Jekeli (2001). In some cases, even better results are reachable (Wei and Schwarz 1998; Bruton 2000). In a land vehicle-based system, which encounters more disturbances and noise in both the IMU and the GPS observables (usually the airborne scenarios are benign), high-resolution (half wavelength of 2 km) gravity estimates are obtained by Li and Jekeli (2008) with 1–3 mGal down component precision and 5–9 mGal horizontal precision.

These reported precisions and resolutions do not only depend on the methods employed in the data processing, but also largely based on the performance of the IMUs, the speed and the altitude of the aircraft, and the quality of the positioning solution; see Hannah (2001) report for a detailed discussion on this topic. In general, a successful high-resolution SINS/DGPS gravimetric survey requires high-quality navigation-grade IMUs, low flight altitudes, and a moderate

velocity as well as precise (cm-level) position solution. However, these ideal configurations may not be always available or achievable in practice. It is worthwhile to carry out new studies to investigate the possibility of detecting gravity signals with reasonable accuracies from relatively weak (in terms of gravimetry) observation systems, especially where the low-cost IMUs are used. Because their relatively low prices, in practice, these low-grade IMU are more often used for attitude determination, despite their high level of noise. As such, even if they can only obtain good estimates in certain frequency bands, it is still beneficial to the physical geodesy community who desperately needs gravity data to better understand the shape and subsurface structure of the Earth.

For this purpose, we investigate both a navigation-grade and a tactical-grade IMU data collected during the GLS06 campaign over the northern Gulf of Mexico, conducted jointly with the Naval Research Laboratory. Section 2 briefly introduces the method of SINS/DGPS vector gravimetry. The data processing and results are given in Sect. 3. Finally, a discussion and some conclusions are given in Sect. 4.

2 The method of INS/GPS vector gravimetry

Because the accelerometer only measures the specific forces that are directly applied on it, such as lifting and dragging, the gravitational force is retrievable from the total accelerations that are computed from the GPS positioning solution. In a "quasi-inertial frame", or i-frame (Jekeli 2000), which is Earth-centered and free-falling around the Sun, the gravitational vector of the Earth system, $\mathbf{g}^i$, is given by Eq. (1):

$$\mathbf{g}^i = \ddot{\mathbf{X}}^i - \mathbf{a}^i, \tag{1}$$

where $\mathbf{X}^i$ is the positioning solution in the i-frame, and $\ddot{\mathbf{X}}^i$ can be computed from the GPS positioning solution $\mathbf{X}$ as shown in Eq. (2):

$$\ddot{\mathbf{X}}^i = \frac{\partial^2}{\partial t^2}\mathbf{X}^i = \frac{\partial^2}{\partial t^2}\left(C_e^i \mathbf{X}\right), \tag{2}$$

where C_e^i is the transformation matrix from the Earth Center and Earth fixed frame, e-frame, to the i-frame. After neglecting the nutation, precession, and polar motion of the Earth, $C_e^i = R_3\left(-\omega_e t\right)$, R_3 is a rotation matrix around the z-axis (see Jekeli 2000 for the specifications), ω_e is the rotation rate of the Earth, and t denotes the Greenwich sidereal time, relatively to the initial epoch of the flight.

The dynamic acceleration, $\mathbf{a}^i$, in Eq. (1) can be computed by Eq. (3):

$$\mathbf{a}^i = C_e^i C_n^e C_b^n \mathbf{a}, \tag{3}$$

where $C_n^e = R_3\left(-\lambda\right) R_2\left(\frac{\pi}{2} - \phi\right)$ is the transformation matrix from the navigation frame (North-East-Down), n-frame, to the e-frame; $C_b^n = R_3\left(-\alpha\right) R_2\left(-\chi\right) R_1\left(-\eta\right)$ is the transformation matrix from the platform's body frame, b-frame, to the n-frame; R_1 and R_2 are the rotation matrices around the x-axis and y-axis, respectively (also see Jekeli 2000 for the specifications); ϕ and λ are the platform's geodetic coordinates; η, χ, and α are the attitude angles (roll, pitch, and yaw) determined from the raw observables of the gyros (see Jekeli 2000 for the detailed computations).

Equations (1)–(3) cannot be used directly to compute the gravitational acceleration because the noise in the INS measurements and the errors in kinematic GPS solutions are usually about several thousand times bigger than the required accuracy of the gravity signal, which is on the mGal (10^{-5} m/s^2) level. In addition to the low signal-to-noise ratio, there are many constituents in the noise. It is not a trivial task to remove or reduce all of them. Usually, the noise is supposed to be a combination of random noise and systematic errors. The former is reduced by a low-pass filter, which assumes that high-frequency signal is noise. Though random noise may not only reside in high frequencies and high-frequency signal is not always noise, the low-pass filter is much more efficient than other methods such as some ARMA (Autoregressive and Moving Average) models, which need very high orders (>100) to represent the noise (Li 2007). The systematic errors from the gyros and accelerometers are usually estimated by predetermined models through a sequential least squares adjustment (Li 2007) in the SINS/DGPS dynamic system, which is equivalent to the well-known Kalman filter technique, whose system dynamics are shown in Eq. (4) [see Kwon and Jekeli (2001) and Jekeli (2000) for the derivations].

$$\begin{bmatrix} \dot{\mathbf{b}}_a \\ \dot{\mathbf{b}}_g \\ \dot{\mathbf{k}}_a \\ \dot{\mathbf{k}}_g \\ \dot{\boldsymbol{\psi}}^i \end{bmatrix} = \begin{bmatrix} \mathbf{0} & \mathbf{0} & \mathbf{0} & \mathbf{0} & \mathbf{0} \\ \mathbf{0} & \mathbf{0} & \mathbf{0} & \mathbf{0} & \mathbf{0} \\ \mathbf{0} & \mathbf{0} & \mathbf{0} & \mathbf{0} & \mathbf{0} \\ \mathbf{0} & \mathbf{0} & \mathbf{0} & \mathbf{0} & \mathbf{0} \\ \mathbf{0} & -C_b^i & \mathbf{0} & -C_b^i\left[\boldsymbol{\omega}_{ib}^b\right] & \mathbf{0} \end{bmatrix} \begin{bmatrix} \mathbf{b}_a \\ \mathbf{b}_g \\ \mathbf{k}_a \\ \mathbf{k}_g \\ \boldsymbol{\psi}^i \end{bmatrix} + \begin{bmatrix} \mathbf{0} & \mathbf{0} & \mathbf{0} & \mathbf{0} & \mathbf{0} \\ \mathbf{0} & \mathbf{0} & \mathbf{0} & \mathbf{0} & \mathbf{0} \\ \mathbf{0} & \mathbf{0} & \mathbf{0} & \mathbf{0} & \mathbf{0} \\ \mathbf{0} & \mathbf{0} & \mathbf{0} & \mathbf{0} & \mathbf{0} \\ \mathbf{0} & \mathbf{0} & \mathbf{0} & \mathbf{0} & -C_b^i \end{bmatrix} \begin{bmatrix} \mathbf{0} \\ \mathbf{0} \\ \mathbf{0} \\ \mathbf{0} \\ \boldsymbol{\epsilon}_g \end{bmatrix} \tag{4}$$

where $\mathbf{b}_a$ is the accelerometer bias, $\mathbf{b}_g$ is the gyro bias, $\mathbf{k}_a$ and $\mathbf{k}_g$ are the scale factor errors for the accelerometers and the gyros, C_b^i is the transformation matrix from the b-frame to the i-frame, $\boldsymbol{\psi}^i$ is the orientation error, $\boldsymbol{\omega}_{ib}^b$ is the angular rate of the b-frame with respect to the i-frame, the operator $\left[\boldsymbol{\omega}_{ib}^b\right]$ is a diagonal matrix with diagonal elements from $\boldsymbol{\omega}_{ib}^b$, and $\boldsymbol{\epsilon}_g$ is the random noise of the gyro.

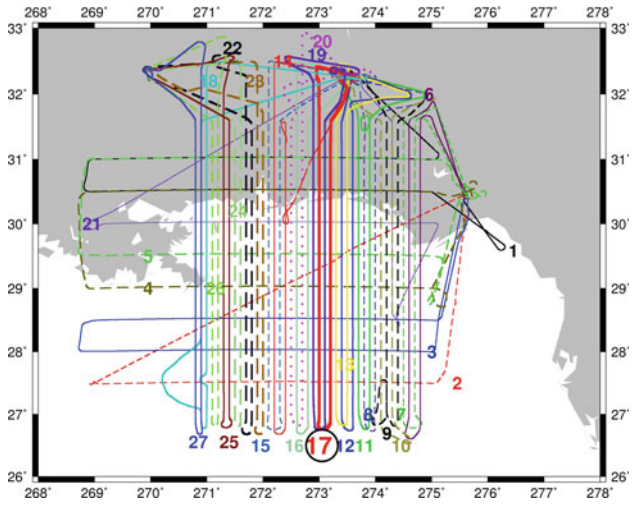

Fig. 1 The flight trajectory of the GLS2006 data

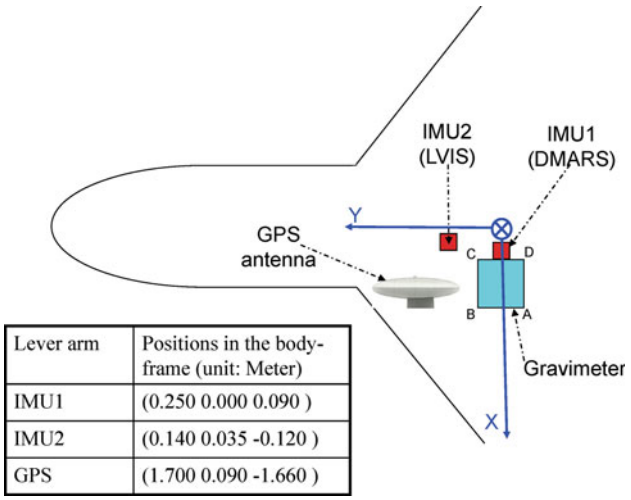

Lever arm	Positions in the body-frame (unit: Meter)
IMU1	(0.250 0.000 0.090)
IMU2	(0.140 0.035 -0.120)
GPS	(1.700 0.090 -1.660)

Fig. 2 The system configuration of the GLS06

These estimated errors are then removed from the observations to yield an estimation of the gravity disturbance, which is given by Eq. (5); see Kwon and Jekeli (2001) for the derivations.

$$\delta \mathbf{g}^n = C_i^n \delta \mathbf{g}^i = C_i^n \left(\mathbf{g}^i - \mathbf{f}^i - \boldsymbol{\gamma}^i - \mathbf{H}\hat{\boldsymbol{\xi}} \right), \tag{5}$$

where $\boldsymbol{\gamma}^i$ is the normal gravity in the i-frame, $\mathbf{f}^i$ is the centrifugal acceleration in the i-frame, $\mathbf{H}$ is the observation matrix that is given by Eq. (6), and $\hat{\boldsymbol{\xi}}$ is the state vector in Eq. (4) that contains the estimated systematic errors, i.e., $\hat{\boldsymbol{\xi}} = [\,\hat{\mathbf{b}}_a\ \hat{\mathbf{b}}_g\ \hat{\mathbf{k}}_a\ \hat{\mathbf{k}}_g\ \hat{\boldsymbol{\psi}}^i\,]$.

$$\mathbf{H} = \left[-C_b^i \ \mathbf{0} \ -[\mathbf{a}]\, C_b^i \ \mathbf{0} \ -\mathbf{a}^i \times \right], \tag{6}$$

where $[\mathbf{a}]$ is a diagonal matrix with diagonal elements from $\mathbf{a}$, $\mathbf{a}^i \times$ is a skew-symmetric matrix (Jekeli 2000), which is given by

$$\mathbf{a}^i \times = \begin{bmatrix} 0 & -a_3^i & a_2^i \\ a_3^i & 0 & a_1^i \\ -a_2^i & a_1^i & 0 \end{bmatrix}.$$

The system dynamics described in Eq. (4) only captures the linear parts of the systematic errors. It is very challenging to fully represent all the systematic errors by direct modeling. To avoid the difficulties of modeling these systematic errors, a Monte Carlo base artificial neural network (Li 2009) could be designed to directly estimate the gravity disturbances. However, large amount of control data sets are required in its training stage, which may prevent us from having a clear understanding of the performances of the IMU. Considering all these reasons, the Kalman system described in Eqs. (4)–(6) is used in this study.

3 Data processing

In the GLS06 campaign, GPS, aerogravity, and INS data were collected over the northern Gulf of Mexico (see Fig. 1). A GPS receiver and a LaCoste–Romberg Air–Sea gravimeter were onboard for obtaining positioning and gravity data, respectively. A navigation-grade strapdown INS (IMU1) and a tactical-grade INS (IMU2) were "originally" used for the purpose of attitude computation (Note: the bias stability and scale factor error of IMU1 is about 1 magnitude better than the specifications of IMU2). Figure 2 gives an intuitive sketch of the instruments' configuration in the aircraft's body frame. In this study, we will investigate both the IMU1 and IMU2 data for gravity determination, instead. Because the IMUs are very close to the onboard gravimeter, this configuration provides a very good opportunity to assess the accuracy of the gravity data derived from the SINS/DGPS gravimetric system. The head-to-head comparisons between the gravimeter and the SINS/DGPS give a very clear evaluation that is not subject to errors from interpolations or upward/downward continuations, which are encountered in previous studies (Jekeli and Li 2006; Li 2010).

Figure 1 shows that there are totally 27 flights in this campaign, which generate a 10-km cross track resolution in the survey area. Each flight has approximately 140 m/s speed at about 11 km altitude. Except some unknown problems (probably in the operational aspects) in flights 1, 22, and 23, all the other flights were problem-free. The onboard GPS and IMU have 2 and 200 Hz sampling rate, respectively. Considering the relatively long flight trajectories, multi-base stations (both the temporary base stations in this campaign and the nearby CORS stations) are used to obtain the best positioning solution of the phase center of the onboard antenna, from which the epoch by epoch position of the IMU is derived by $\mathbf{X}_{\mathrm{IMU}}^i = \mathbf{X}_{\mathrm{GPS}}^i + C_b^i \mathbf{b}$, where the transformation

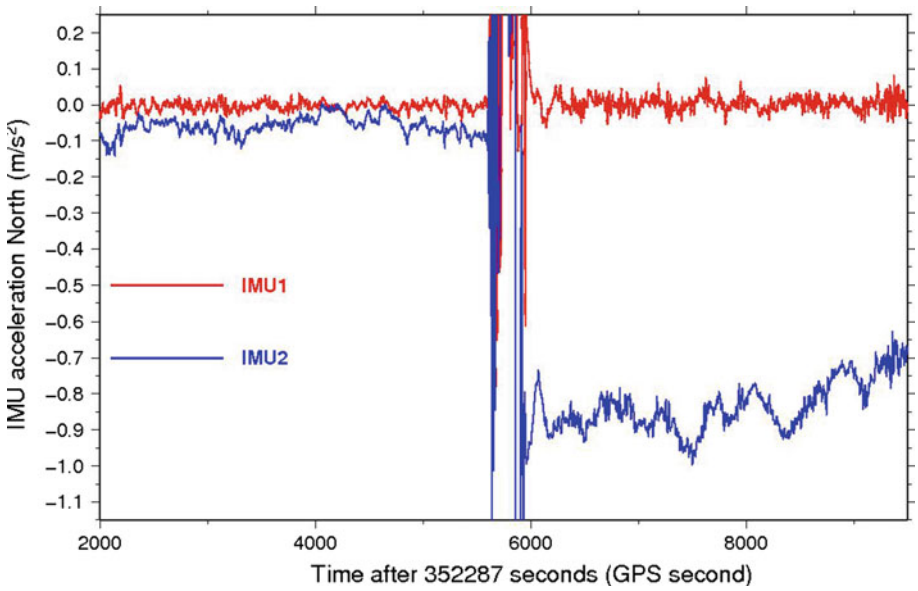

Fig. 3 The IMU-measured dynamic acceleration in north direction

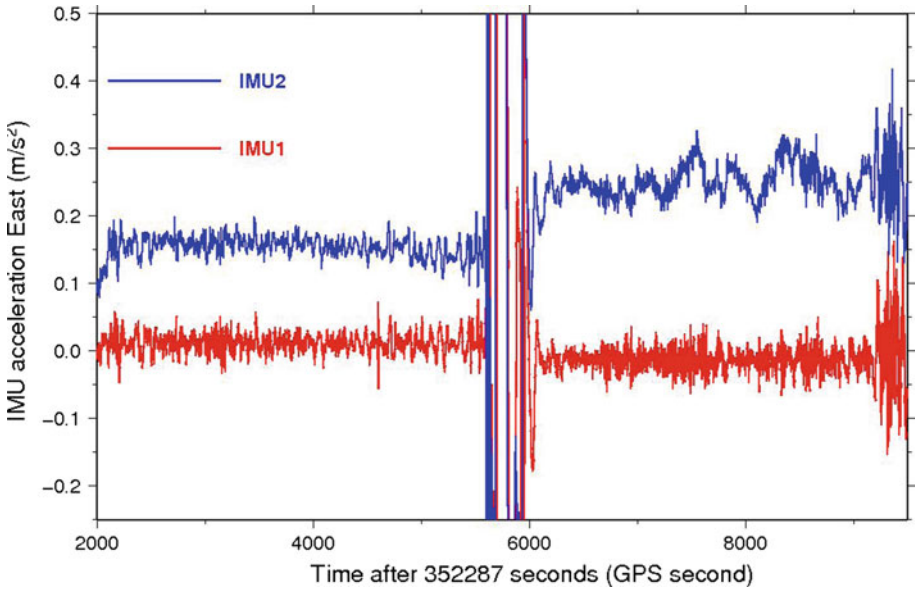

Fig. 4 The IMU-measured dynamic acceleration in east direction

matrix (from the b-frame to the i-frame) C_b^i can be computed from the IMU measurements, and **b** is a vector in the b-frame from the GPS antenna to the center of the IMU. Thus, the lever arm acceleration is eliminated in this study. To keep the focus on gravity estimation, the details of the GPS data processing are not included here.

A typical data set from flight 17 is used to illustrate the processing schemes. First, the IMU-measured velocity increments and angular increments are used to compute the b-frame dynamic acceleration **a**, and the transformation matrix C_b^n in Eq. (3), respectively. Then this acceleration is transformed into the i-frame by using Eq. (3). The IMU-measured accelerations (transformed into n-frame for a better view) are shown in Figs. 3, 4, and 5. It is obvious that there are more oscillations in the tactical-grade IMU (IMU2, blue curves in Figs. 3, 4, 5) derived accelerations than those of the navigation-grade IMU (IMU1, red curves in Figs. 3, 4, 5). Moreover, there are large systematic bias jumps in IMU2 accelerations after high dynamics, such as turns. In general, the oscillations of the blue curves in the second segment (6,000–9,500 s) are much larger than the corresponding in the first segment 2,000–5,500, which shows that the tactical IMU has relatively weak long-term stability. The total kinematic acceleration of the aircraft in this i-frame is obtained by taking two consecutive derivatives of the positioning solution obtained from GPS. The results are shown in Figs. 6, 7, and 8. In Figs. 3, 4, 5, 6, 7, and 8, the spikes and oscillations at the beginning and the end of the flight are removed because the high dynamics of the aircraft in the taking off and landing periods make it very difficult to accurately determine the gravity data. The large acceleration oscillations in the middle of these figures (Figs. 3, 4, 5, 6, 7, 8) are due to the turns of

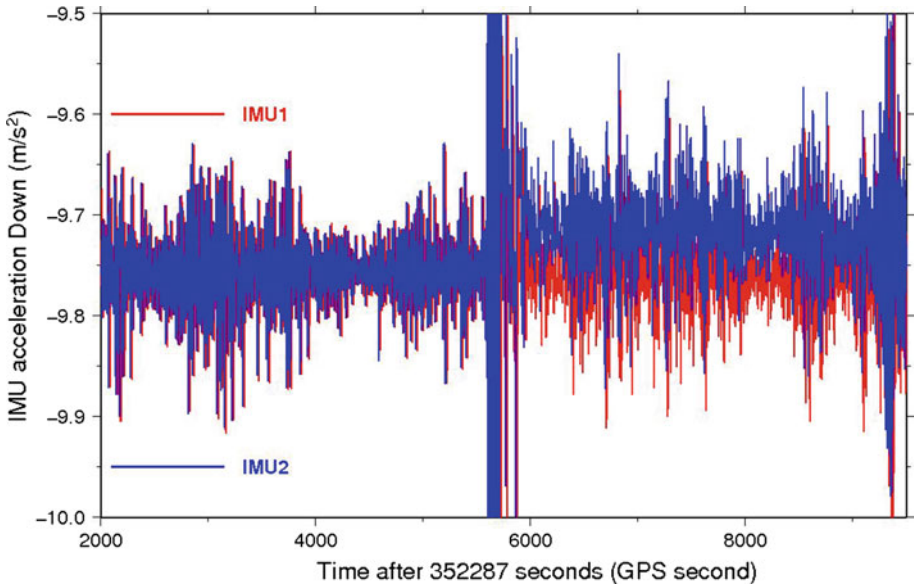

Fig. 5 The IMU-measured dynamic acceleration in down direction

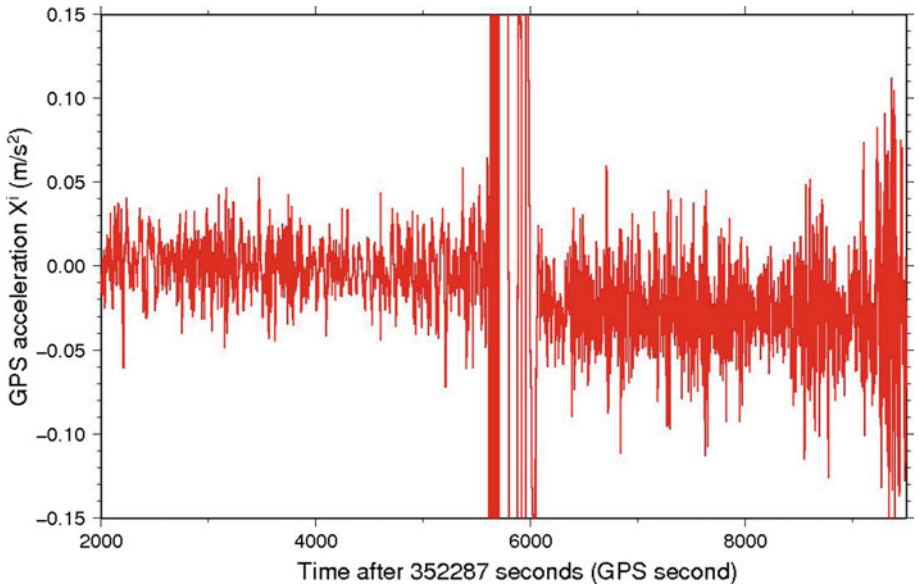

Fig. 6 The GPS-derived totally kinematic acceleration along the x-axis of the i-frame

the aircraft (because it has to be parked on land; see Fig. 1). Also no useful gravity data can be obtained in this period of time. Thus, only the data in the middle parts are used to estimate the gravity disturbances. As a result, for each flight, usually, we have two parts of gravity estimates. One is from the outbound track, and the other is from the returning track.

The magnitude of the gravity disturbances, usually in hundreds of mGals, is about several thousand times smaller than the magnitudes of the oscillation in the accelerations. The useful gravity signal is hiding deeply in the raw observations. This is the so-called low-SNR (signal-to-noise ratio) problem. Therefore, an efficient de-noising approach should be employed to separate the observation noise from the real signal. To have a more clear understanding of the noise distribution in the accelerations, a spectral analysis is applied. Figures 9 and 10 show the power spectrum density (PSD) of the GPS and the INS acceleration, respectively. It is clear that the power distributions are very complicated in the middle- to high-frequency bands (>10^{-3} Hz). For the IMU-measured dynamic accelerations, the PSD of the navigation-grade IMU acceleration is decreasing more quickly than the PSD of the tactical-grade IMU acceleration in the low-frequency band (8.2×10^{-5}–10^{-3} Hz), which implies that in the time domain the former is smoother (less oscillation) than the latter. In the middle-frequency band [10^{-3}–$10^{-0.3}$ Hz], the PSDs of both these IMU-derived accelerations are very similar. It is obvious that the power of the navigation-grade IMU is much less than the power of the tactical-grade IMU in the high-frequency band ($10^{-0.3}$–10^{2} Hz], where the noise is usually supposed to reside in. Experimental tests show

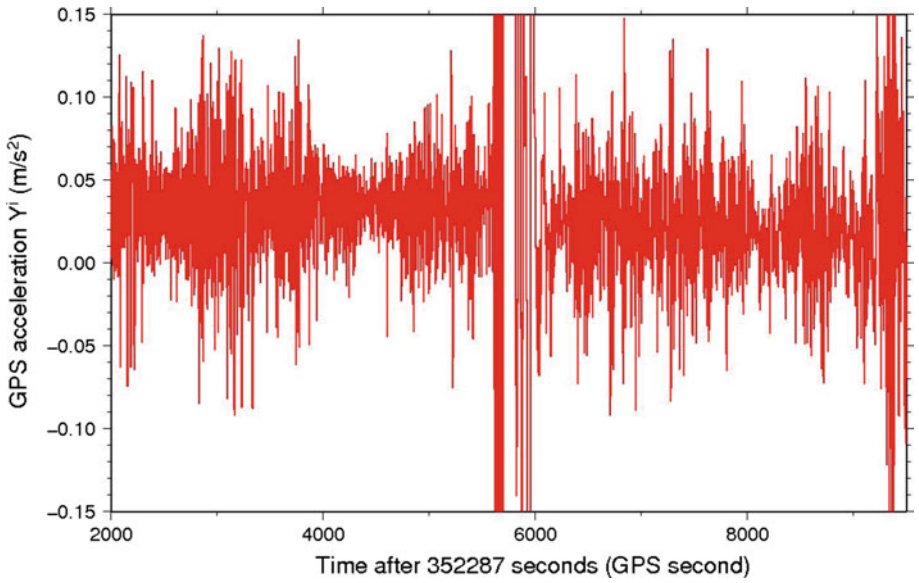

Fig. 7 The GPS-derived totally kinematic acceleration along the y-axis of the i-frame

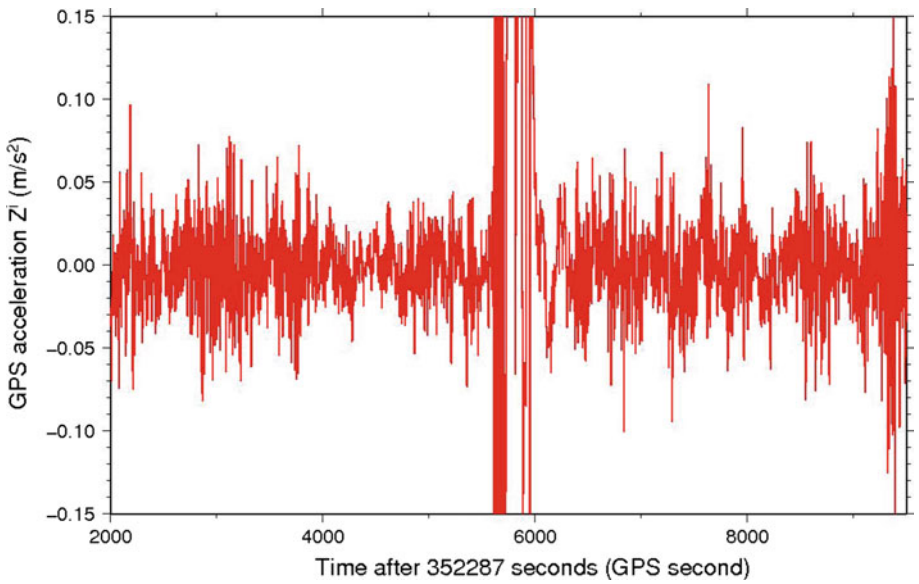

Fig. 8 The GPS-derived totally kinematic acceleration along the z-axis of the i-frame

that we have to use a 240s smoother to remove the random noise before applying Eq. (4) to reduce the systematic errors. Because of the limitations of Eq. (4) in representing the system dynamics, usually there are left-over systematic effects in Eq. (5). These remaining errors are removed by an end-point matching technique, which removes the bias and trend by comparing the gravity disturbance estimates with the upward continued control data at both the beginning and the end of each track; see Li (2007) for more details. The final estimates of the gravity disturbances are shown in Fig. 11.

To assess the accuracies of these results, Fig. 11 also shows the "control" data obtained from various sources. In the horizontal component, both the local model such as DEFLEC 99 (Smith and Roman 2001) and the global model such as EGM2008 (Pavlis et al. 2008) can be used as a reference. However, the contribution from the curvature of the plume line needs to be properly handled if the former is employed. For simplicity, the EGM2008 coefficient model is applied to compute the horizontal component directly at the flight height. Large discrepancies are observed between the estimated horizontal components and the model predicted ones. This shows that the north and east components estimated from this system have poor accuracies.

The down component, which is often used in local geoid computations, is compared to the onboard gravimeter measured values and to the upward continued surface control data from NGS database (Wang et al. 2008). The differences and their standard deviations are shown in the right bottom side of Fig. 11, from which we see very good (<2 mGal) agreements. On the other hand, the gravity disturbance estimates from the tactical-grade IMU (IMU2 in Fig. 2) oscillates around the "true" data indicated by the gravimeter with about

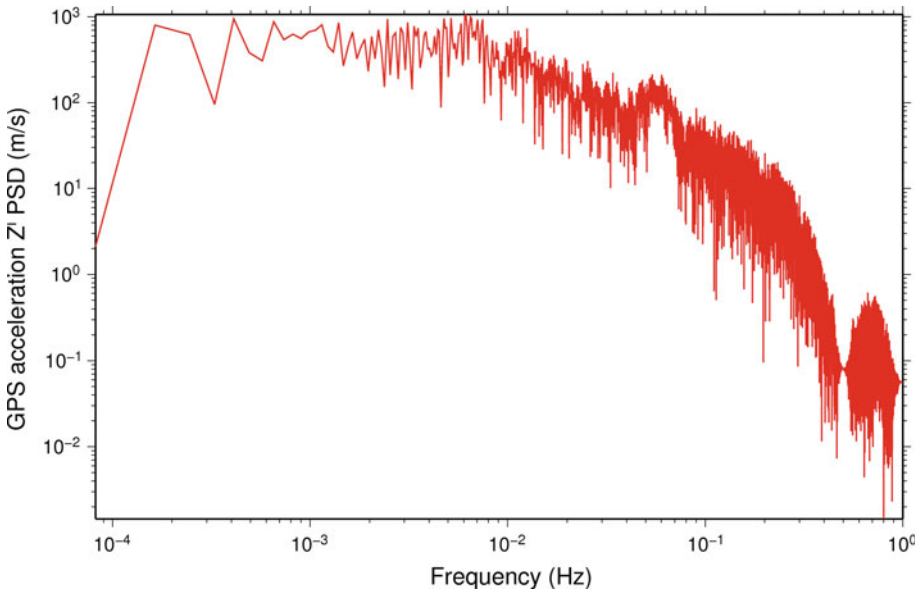

Fig. 9 The power spectrum density of the GPS acceleration along the z-axis of the i-frame (The other components in the x- and y-axes have similar characteristics. To save space, they are not plotted here)

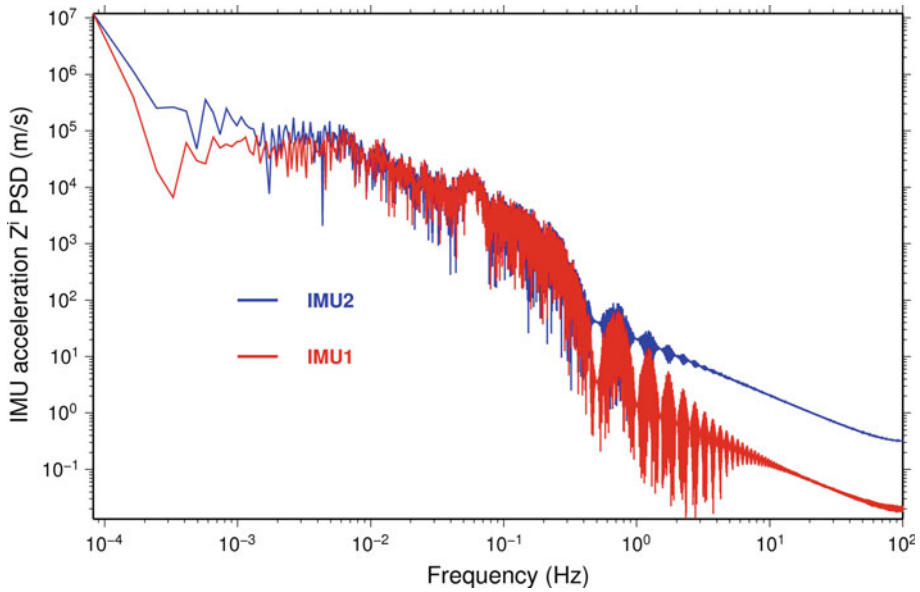

Fig. 10 The power spectrum density of the IMU acceleration along the z-axis of the i-frame (The other components in the x- and y-axes have similar characteristics. To save space, they are not plotted here)

15 mGal amplitude. The precision of the IMU2-measured gravity disturbance is 7.72 and 7.85 mGal as compared to the upward continued control data and the gravimeter's measurements. Obviously, this precision level is not acceptable for precise geodetic applications. Therefore, the question arises whether there are any frequency bands where the tactical-grade IMU contribution is useful? To test this possibility, the total energy of the errors (defined as the observed minus the control data) in the space domain are partitioned into several frequency bands according to Eq. (7).

$$\left[STD_{F1}^{F2}\right]^2 = \frac{1}{T}\frac{\Delta t}{2N}\left(\sum_{m1}^{m2}(G_\tau)_n\left(G_\tau^*\right)_n + \sum_{2N-m2+1}^{2N-m1+1}(G_\tau)_n\left(G_\tau^*\right)_n\right), \tag{7}$$

where T is the total length of the track (208.46 km), Δt is the sampling interval (140 m), $2N$ is the total number of the sampling points, G_τ is the bias-free Fourier transform of the gravity disturbance error estimates, $F1$ and $F2$ are the frequency boundaries, $m1 = F1 \cdot 2N\Delta t$, and $m2 = F2 \cdot 2N\Delta t$; see Li and Jekeli (2006) for more details.

The standard deviations (STD_{F1}^{F2}) of the error in the corresponding frequency band $[F1 - F2]$ is given in Table 1, which shows that in the long wave length ($\geq$125 km), we can still obtain less than 3 mGal precisions from the tactical-grade IMU. Figure 11 only shows the outbound part of flight 17. In the returning track, the oscillations of the tactical-grade IMU-estimated gravity data are up to several hundred mGals, primarily because the relatively large oscillations in the IMU2-measured accelerations; see the second segment of the blue curve in Figs. 3, 4, and 5.

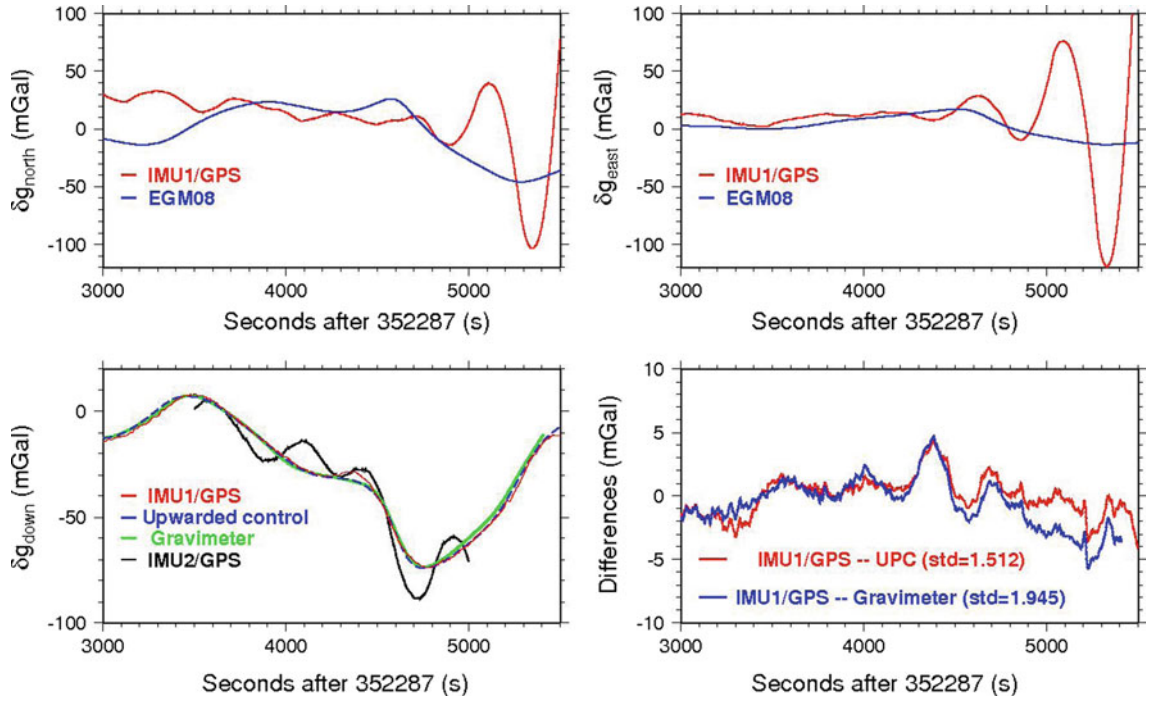

Fig. 11 The estimated gravity disturbances and their comparisons (In the horizontal components, the estimates are compared with EGM08. In the down component, the estimates are compared with both the upward continued control and the onboard gravimeter. The corresponding differences are shown in the *right bottom* panel. To save space, this plot only shows the results from the outbound track of this flight. The horizontal components gravity estimates from IMU2 are not included because large oscillations in the order of 1,000 mGal.)

Table 1 The precisions of the gravity disturbance derived from the tactical-grade INS in the frequency domain

$F1$ (cycle/km)	$F2$ (cycle/km)	IMU2/DGPS-UPC (mGal)	IMU2/DGPS-gravimeter (mGal)
0.00	1/T	0.00	0.00
1/T	1/125	2.29	2.59
1/125	1/100	4.01	4.14
1/100	1/75	0.00	0.00
1/75	1/50	5.13	5.09
1/50	1/25	3.36	3.36
1/25	1/10	0.67	0.71
1/10	$1/f_n$	0.29	0.34
$1/\infty$	$1/f_n$	7.72	7.85

f_n Nyquist frequency

Following the same procedure, all the other successful flights in Fig. 1 are processed. Figure 12 shows the statistics of the differences between the down component of the navigation-grade IMU and the upward continued control as well as the gravimeter measured data at exactly the same position. Compared with the upward continued control, all the statistics have better than 3 mGal precision, except the returning track of flight 18 whose precision is 3.766 mGal. Notice that because the control data are used in the end-point matching step, there is no bias left in the estimates. Compared with the onboard gravimeter's measurements, the precision also shows very good (<3.2 mGal) agreement in most of the time, except only one case (outbound track of flight 21 where the upward continued control also has large differences with the gravimeter's output). The SINS/DGPS-derived gravity signals are clearly precise and could be valuable for geoid computations.

4 Discussions and conclusions

Two grades of IMU are used in the strapdown INS/DGPS gravimetric system in an airborne scenario. The acceleration data computed from both of the IMUs have large oscillations. In addition, there are noticeable systematic jumps in the tactical-grade IMU-measured accelerations. Spectral analysis shows that the noise is primarily residing in the middle- to high-frequency band. A relatively large (240 s) smoother window is applied to reduce the noise. The systematic errors of the IMU are estimated by using the modified Kalman Filter (Kwon and Jekeli 2001). The left over trend and bias in the gravity disturbance estimates are removed by using the end-point matching method. The 27 flights of the GLS06 campaign yield 44 successful gravity profiles. Except only one

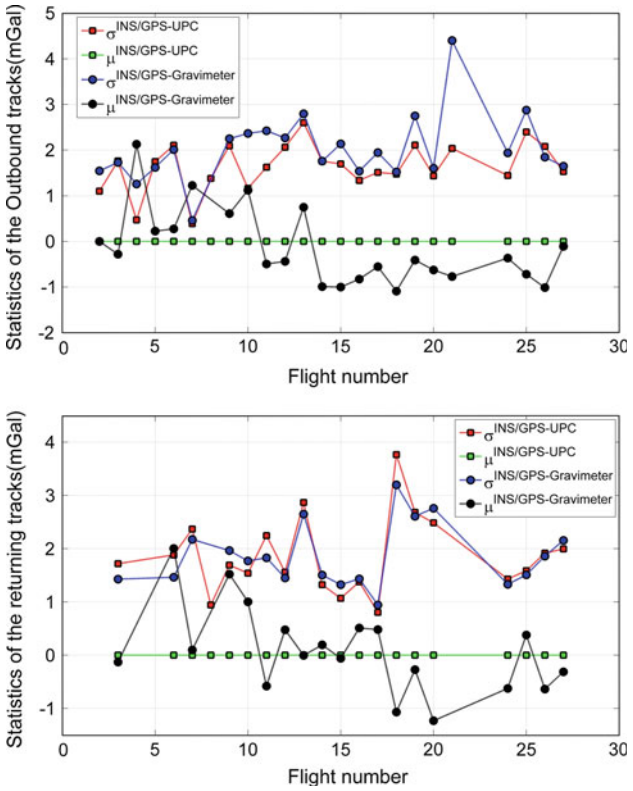

Fig. 12 The statistics of the differences between the down component of the navigation-grade IMU and the upward continued control as well as the gravimeter measured data at exactly the same position

profile out of the total 44 tracks, the system derived down component gravity disturbances from the navigation-grade IMU have better than 3 mGal precision agreement with the upward continued control data. Compared with the onboard gravimeter, the precision ranges from 0.5 to 3.2 mGal. The precision is very close to the claimed precision range (1–2 mGal) of the gravimeter. However, the low-grade IMU only provides good (std $<$ 3 mGal) estimates in longer (125–208 km) wavelength. Even though the aircraft's high altitude (11 km) and fast speed (140 m/s) provide a relatively stable environment, a large (240 s) smoothing window has to be applied to yield these results. Consequently, the gravity estimates have an averaged 34 km along-track resolution, which is coarser than the designed 10 km spatial resolution. Unlike the gravimeter, which only provides the down component gravity disturbance, the SINS/DGPS system also offers the horizontal components of the gravity disturbances. However, the results show large differences from the model predicted values. Other techniques such as the neural network (Li 2009) may be applied to yield better results. Though not mentioned too much on the GPS part in this study, the extremely long baselines also cause detrimental effects on the precision of the gravity disturbance estimates.

Acknowledgments The author would like thank Dr. Roman, Dr. Wang, and Mr. Saleh at the National Geodetic Survey for preparing the data and polishing the English. The author also would like to thank reviewer 1 of this paper for the valuable comments.

References

Bruton A (2000) Improving the accuracy and resolution of SINS/DGPS airborne gravimetry. PhD thesis, Department of Geomatics Engineering, University of Calgary, Calgary, UCGE Report No. 20145

Hannah J (2001) Airborne gravimetry: a status report. Department of Surveying, University of Otago, Dunedin

Jekeli C (2000) Inertial navigation systems with geodetic applications. Walter de Gruyter, Berlin

Jekeli C, Li X (2006) INS/GPS vector gravimetry along roads in Western Montana. The Ohio State University Report No. 477

Kwon JH, Jekeli C (2001) A new approach for airborne vector gravimetry using GPS/INS. J Geod 74(10):690–700

Li X, Jekeli C (2006) INS/GPS vector gravimetry assessment using repeated traverses in Montana. In: Proceedings of 1st international symposium of the international gravity field service, Istanbul, Turkey, pp 31–36

Li X (2007) Moving base INS/GPS vector gravimetry on a land vehicle. PhD dissertation, OSU report 486

Li X, Jekeli C (2008) Ground-Vehicle INS/GPS Gravimetry. Geophysics 73(2):I1–10

Li X (2009) Comparing the Kalman filter with a Monte Carlo-based artificial neural network in the INS/GPS vector gravimetric system. J Geod 83(9):797–804

Li X (2010) Interpolating surface gravity data for assessing the accuracy of a ground INS/GPS gravimetric system. J Survey Eng 136(3):139–146. doi:10.1061/(ASCE)SU.1943-5428.0000025

Pavlis NK, Holmes SA, Kenyon SC, Factor JK (2008) An earth gravitational model to degree 2160: EGM2008. European Geosciences Union General Assembly, Vienna

Schwarz KP (2006) Simultaneous determination of position and gravity from INS/DGPS, Wissenschaftliche Arbeiten der Fachrichtung Geodaesie und Geoinformatik der Universitaet Hannover, Hannover, vol 258, pp 141–148

Smith DA, Roman DR (2001) GEOID99 and G99SSS: 1-arc-minute geoid models for the United States. J Geod 75(9–10):469–490

Wang YM, Roman DR, Saleh J (2008) Analytical downward and upward continuation based on the method of domain decomposition and local functions. In: 6th Hotine-Marussi symposium on theoretical and computational geodesy, vol 132, Part IV, pp 356–360

Wei M, Schwarz KP (1998) Flight test results from a strapdown airborne gravity system. J Geod 72:323–332